Frontiers of Information Technology & Electronic Engineering
www.jzus.zju.edu.cn; engineering.cae.cn; www.springerlink.com
ISSN 2095-9184 (print); ISSN 2095-9230 (online)
E-mail: jzus@zju.edu.cn

Efficient scheme of low-dose CT reconstruction using TV minimization with an adaptive stopping strategy and sparse dictionary learning for post-processing*

Yong DING†, Tuo HU

(*College of Information Science and Electronic Engineering, Zhejiang University, Hangzhou 310027, China*)

†E-mail: dingy@vlsi.zju.edu.cn

Received Apr. 30, 2017; Revision accepted Aug. 9, 2017; Crosschecked Dec. 22, 2017

Abstract: Recently, low-dose computed tomography (CT) has become highly desirable because of the growing concern for the potential risks of excessive radiation. For low-dose CT imaging, it is a significant challenge to guarantee image quality while reducing radiation dosage. Compared with classical filtered backprojection algorithms, compressed sensing-based iterative reconstruction has achieved excellent imaging performance, but its clinical application is hindered due to its computational inefficiency. To promote low-dose CT imaging, we propose a promising reconstruction scheme which combines total-variation minimization and sparse dictionary learning to enhance the reconstruction performance, and properly schedule them with an adaptive iteration stopping strategy to boost the reconstruction speed. Experiments conducted on a digital phantom and a physical phantom demonstrate a superior performance of our method over other methods in terms of image quality and computational efficiency, which validates its potential for low-dose CT imaging.

Key words: Low-dose computed tomography (CT); CT imaging; Total variation; Sparse dictionary learning
https://doi.org/10.1631/FITEE.1700287 **CLC number:** TP391.41

1 Introduction

Computed tomography (CT) has become a significant diagnostic imaging modality. In a standard CT scan, an X-ray source spins around a patient and a detector is used to receive X-ray intensity data (so-called projections) at different positions. Then in the reconstruction process, the cross-sectional image is computed from raw projections using a reconstruction method, such as the clinical standard filtered backprojection (FBP) (Ginat and Gupta, 2014). Recently, there has been increasing concern that excessive radiation exposure in CT scanning may have relations to the increased cancer risks of the patient. As a straightforward and efficient way to alleviate this negative effect, low-dose CT has become highly desirable. Low-dose CT scanning is usually performed by lowering the X-ray tube load setting or by decreasing the number of projections, leading to noisy or insufficient projection data. It is a significant challenge to maintain image quality while reducing radiation dose. Unfortunately, researchers have found that images reconstructed from low-dose data using FBP suffer from heavy noise and artifacts (Yan *et al.*, 2012). Conventional iterative reconstruction, such as the simultaneous algebraic reconstruction technique (SART) (Anderson and Kak, 1984), also cannot improve image quality degradation in low-dose CT. There has been an urgent need to develop dedicated method for low-dose CT reconstruction.

In the past decade, compressed sensing (CS) has attracted much research interest and revealed powerful performance in many problems including sparse

* Project supported by the National High-Tech R&D Program (863) of China (No. 2015AA016704c) and the Zhejiang Provincial Natural Science Foundation, China (No. LY14F020028)

ORCID: Yong DING, http://orcid.org/0000-0002-5226-7511

sampling and signal and image reconstruction (Lustig *et al.*, 2008). According to the CS theory, sparse signals can be restored from significantly fewer samples other than are required by the Nyquist sampling theorem (Candes *et al.*, 2006). Although the CT image is not sparse in general, it is found to have a sparse representation after being converted by some transforms, such as the discrete gradient transform (DGT) (Xu *et al.*, 2012). This means that the CS theory can be applied to low-dose CT imaging; i.e., it is possible to reconstruct fine enough images from fewer projections. Furthermore, for the clinical application of low-dose CT, the CS theory brings new hope by safely reducing CT scan dose with guaranteed image quality (Park *et al.*, 2012).

Motivated by the CS theory, many CS-based methods have been developed and they have generated a breakthrough in low-dose reconstruction (Yan *et al.*, 2012). Generally, these CS-based methods use the framework of iterative reconstruction and modify it by incorporating a prior known image property. Total variation (TV, i.e., the sum of DGT coefficients) has become a more popular prior knowledge than others such as tight frame (TF) regularization (Jia *et al.*, 2011) and soft-thresholding (Yu and Wang, 2010). The TV prior knowledge is based on the piecewise constant property (sparsity in DGT domain, mathematically) of a CT image, indicating that the image should have a small TV value. In practice, TV-based methods, such as adaptive-steepest-descent projection onto convex sets (ASD-POCS) (Sidky *et al.*, 2008), reconstruct the CT image by solving a TV minimization problem, using iterative optimization to look for a TV-minimal solution. Compared with conventional FBP algorithms, TV-based iterative reconstruction has achieved superior results under low-dose protocols. However, CS iterative reconstruction is unfortunately prone to be computationally intensive, so its clinical application is severely hindered (Yan *et al.*, 2014).

To promote clinical application of the CS-based method for low-dose CT, the reconstruction speed of current methods must be increased. The extensive time requirements of CS-based methods are mainly because so many iterations are needed (each iteration takes nearly the same time as an FBP). Studies show that once a certain level of image quality is reached in iterative optimization, the following iterations are of low efficiency and benefit, but directly discarding them will severely degrade imaging performance (Niu and Zhu, 2012; Niu *et al.*, 2014). This fact motivates us to develop an iteration-reduced method accompanied by some powerful image post-processing to achieve both high computational efficiency and good image quality.

Sparse dictionary learning (SDL) has attracted a lot of attention in recent years. Many researchers have started to investigate SDL for medical imaging including CT reconstruction and magnetic resonance imaging (MRI) (Yuan *et al.*, 2015). Some methods incorporate dictionary learning into an iterative reconstruction framework, such as adaptive dictionary-based statistical iterative reconstruction (ADSIR) (Xu *et al.*, 2012) and 3D dictionary learning (3D-DL) (Liu *et al.*, 2016). Dictionary learning that is implanted into iterative reconstruction in those methods not only helps improve imaging performance, but also increases computational complexity because of nested iterations. Other methods use dictionary learning as post-processing to reduce artifacts in images reconstructed with FBP, such as the artifact-suppressed dictionary learning (ASDL) algorithm (Chen *et al.*, 2014).

In this paper, we present a complementary method for low-dose CT reconstruction. Our goal is to reconstruct fine enough images from low-dose projections, with reduced time overhead compared with CS-based iterative reconstruction. TV minimization is employed to reconstruct an intermediate image, and then sparse coding is used for post-processing to remove the remaining noise and yields a clinically acceptable CT image. Moreover, the computational cost is reduced by properly scheduling these two algorithms using an adaptive stopping strategy. The workflow of the proposed method is shown in Fig. 1. Experimental results demonstrate its power in both image quality and computational efficiency, indicating that it is a promising approach and may serve as a base for future studies of low-dose CT reconstruction.

2 Proposed method

As illustrated in Fig. 1, the proposed method is composed of two operational phases. In Phase 1, TV minimization is executed to reconstruct an

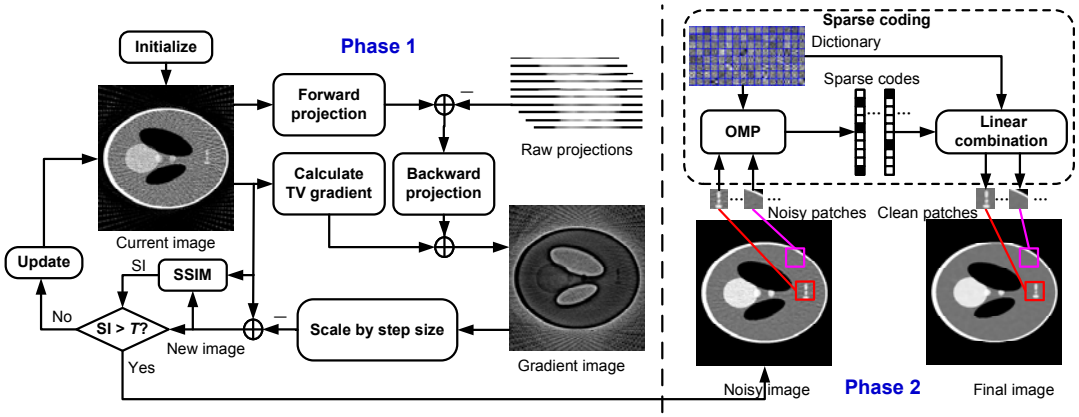

Fig. 1 Workflow of the proposed method
SI: similarity index; TV: total variation; SSIM: structural similarity; OMP: orthogonal matching pursuit

intermediate image. Then in Phase 2, sparse coding, as part of sparse dictionary learning, is used to process the image of Phase 1 and output the final image.

2.1 TV minimization for reconstructing the intermediate image

TV minimization is a kind of CS-based iterative reconstruction. Apart from the analytical model in FBP, iterative methods establish a discrete model where CT scanning is expressed as a linear system, $\boldsymbol{M\mu}=\boldsymbol{b}$, with $\boldsymbol{M}$ being the system matrix whose elements can be calculated using ray tracing algorithms, such as the Siddon algorithm (Siddon, 1985), $\boldsymbol{\mu}$ a vector containing X-ray attenuation coefficients of the patient, and $\boldsymbol{b}$ a vector storing the pixel value of projection data. Here, the CT imaging problem is to calculate X-ray attenuation coefficients $\boldsymbol{\mu}$ using $\boldsymbol{M}$ and $\boldsymbol{b}$, but a straightforward solution is impossible because $\boldsymbol{M}$ is underdetermined in practice. Generally, iterative optimization is used to approximate the exact solution.

TV minimization can be formulated as a constrained optimization problem:

$$\min_{\boldsymbol{\mu}} \|\boldsymbol{\mu}\|_{\mathrm{TV}} \text{ s.t. } \frac{1}{2}\|\boldsymbol{M\mu}-\boldsymbol{b}\|_2^2 \le \varepsilon, \tag{1}$$

where $\|\cdot\|_{\mathrm{TV}}$ is the TV norm, $\boldsymbol{M}$ is used for forward projection, and ε denotes the tolerance of difference between calculated and measured raw projections.

To address this problem efficiently, we transform it into a bounded convex problem using the logarithmic barrier method (Niu and Zhu, 2012; Niu *et al.*, 2014). The object function now consists of a TV term and a data-fidelity term, and its formula can be rewritten as follows:

$$\min_{\boldsymbol{\mu}} \|\boldsymbol{\mu}\|_{\mathrm{TV}} - \ln\left(\varepsilon - \frac{1}{2}\|\boldsymbol{M\mu}-\boldsymbol{b}\|_2^2\right). \tag{2}$$

This minimization problem is then solved by a two-point step size gradient method (Barzilai and Borwein, 1988; Niu and Zhu, 2012). In each iteration, as shown in Phase 1, forward projection, backward projection, and TV transform are applied to calculate the gradient of the object function in Eq. (2). Then this gradient image is used to update $\boldsymbol{\mu}$ after being scaled by a step size.

To reduce iterations by scheduling iterative optimization, it is important to find a proper stopping point. Instead of stopping at a fixed iteration (e.g., at the 100th iteration), we design an adaptive stopping strategy. Specifically, the structural similarity (SSIM) index (Wang *et al.*, 2004), a metric of image quality assessment, is adopted to measure the similarity index (SI) between the image of the current iteration and that of the last iteration. Once the SI reaches a threshold T close to 1; i.e., the two images of adjacent iterations are similar enough, the following iterations will no longer be effective. In this way, the loop will repeat until the SI exceeds the predefined threshold, as we can see in Fig. 1.

2.2 Sparse dictionary learning for post-processing

Subsequently, sparse dictionary learning is employed to eliminate the remaining noise in the TV

minimization output image. Generally speaking, the image denoising problem is to restore the original image from a distorted image composed of desired information and unwanted noise. Image denoising by sparse dictionary learning is based on the assumption that the desired signal can be represented as a linear combination (whose coefficients are so-called sparse code) of a few atoms in an overcomplete dictionary, while noise cannot do (Elad and Aharon, 2006; Dong *et al.*, 2013). Thus, the desired signal is retained while noise is ruled out, once we rebuild the image using its sparse code.

A standard sparse dictionary learning has two steps, dictionary construction and sparse coding. To reduce the execution time, we train an overcomplete dictionary in advance on image patches extracted from the training dataset. Suppose $\boldsymbol{D}\in\mathbb{R}^{n\times m}$ is the dictionary to be learned, and it has m atoms of size n ($n<<m$, for overcomplete); $\boldsymbol{Z}\in\mathbb{R}^{n\times k}$ is the set of those extracted patches, composed of k patches that are reordered as vectors of size n. The dictionary construction can be formulated as

$$\min_{\boldsymbol{D},\boldsymbol{A}}\left\|\boldsymbol{D}\boldsymbol{A}-\boldsymbol{Z}\right\|_{\mathrm{F}}\ \text{s.t.}\ \left\|\boldsymbol{\alpha}_i\right\|_0\le s_0,\forall i, \tag{3}$$

where $\boldsymbol{A}\in\mathbb{R}^{m\times k}$ denotes the set of the sparse codes for patches, $\boldsymbol{\alpha}_i$ is the ith column of $\boldsymbol{A}$, $\|\cdot\|_{\mathrm{F}}$ is the Frobenius norm, and s_0 is the threshold for the number of non-zero elements for every sparse code. We use K-singular value decomposition (K-SVD) to solve this problem and generate a dictionary (Aharon *et al.*, 2006).

Based on the pre-trained dictionary, the image yielded in Phase 1 is then processed using sparse coding in Phase 2. Here, we decompose the intermediate image (vectorized as $\boldsymbol{X}\in\mathbb{R}^N$) into small overlapped patches (vectorized as $\boldsymbol{x}_i\in\mathbb{R}^n$, $n<<N$) and process these patches separately. Each patch is extracted using $\boldsymbol{x}_i=\boldsymbol{E}_i\boldsymbol{X}$, where $\boldsymbol{E}_i\in\mathbb{R}^{n\times N}$ is the extraction matrix for $\boldsymbol{x}_i$ (Elad and Aharon, 2006). For every image patch $\boldsymbol{x}_i$, its sparse code is sought by solving such an error-constrained optimization problem:

$$\boldsymbol{\alpha}_i^*=\arg\min_{\boldsymbol{\alpha}_i}\left\|\boldsymbol{\alpha}_i\right\|_0\ \text{s.t.}\ \left\|\boldsymbol{D}\boldsymbol{\alpha}_i-\boldsymbol{x}_i\right\|_2^2\le\sigma, \tag{4}$$

where σ is the error tolerance. The orthogonal matching pursuit (OMP) algorithm is used to implement this minimization task (Elad and Aharon, 2006). After every optimal sparse code $\boldsymbol{\alpha}_i^*$ is obtained, clean patches are computed by linear combination $\boldsymbol{x}_i^*=\boldsymbol{D}\boldsymbol{\alpha}_i^*$. With these clean patches, the final image is built by solving

$$\boldsymbol{Y}^*=\arg\min_{\boldsymbol{Y}}\lambda\left\|\boldsymbol{X}-\boldsymbol{Y}\right\|_2^2+\sum_i\left\|\boldsymbol{x}_i^*-\boldsymbol{E}_i\boldsymbol{Y}\right\|_2^2, \tag{5}$$

where λ is a penalty factor. In fact, the solution of this quadratic problem can be directly derived as

$$\boldsymbol{Y}^*=\left(\lambda\boldsymbol{I}+\textstyle\sum_i\boldsymbol{E}_i^{\mathrm{T}}\boldsymbol{E}_i\right)^{-1}\left(\lambda\boldsymbol{X}+\textstyle\sum_i\boldsymbol{E}_i^{\mathrm{T}}\boldsymbol{x}_i^*\right), \tag{6}$$

where $\boldsymbol{I}$ is the identity matrix of size $N\times N$ and $\boldsymbol{E}_i^{\mathrm{T}}$ is the transpose of extraction matrix $\boldsymbol{E}_i$. Eq. (6) means that the final image is computed by weighted averaging of the noisy image $\boldsymbol{X}$ and clean patches.

3 Experiments and discussion

3.1 Experimental setup

To evaluate imaging performance of the proposed method, we conducted experiments on the Shepp-Logan digital phantom and the Catphan physical phantom. The projections data of the physical phantom were acquired using a CT scan with 655 projections over 360°. For both phantoms, the CT system has a reconstructed image having a size of 512×512 pixels and a detector of 1024 pixels.

Parameters were selected as follows. In Phase 1, the value of ε was estimated using the Poisson noise of the projection data, derived from the intensity of flat plane $\boldsymbol{I}_0$ (in unit of photon number) and projection $\boldsymbol{b}$ (Niu and Zhu, 2012):

$$\varepsilon=\sum_{i=1}^{N_{\mathrm{d}}}\frac{1}{I_0(i)-\mathrm{e}^{-b(i)}}, \tag{7}$$

where N_{d} is the number of detector pixels. The threshold T of the similarity index was set to 0.9999. In Phase 2, $\boldsymbol{D}$ has a size of 64×256 and was trained on image patches of size n=8×8 extracted from an ideal image dataset. According to our experience, relatively good results can be obtained when λ is set to a value between 2 and 4. Here, we fixed λ at 3.21 empirically.

Results of the proposed method are compared with those of other methods. The first method is FBP, which is employed by most commercial CT scanners. The second method is FBP-BM3D, which first executes FBP for image reconstruction and then processes the reconstructed image by block matching 3D (BM3D) denoising (Dabov *et al.*, 2007), a state-of-the-art image denoising method. The third method is SART, a classical iterative reconstruction. The last method is accelerated barrier optimization compressed sensing (ABOCS), a TV-based iterative reconstruction (Niu *et al.*, 2014).

We also applied numeric metrics for objective assessment. One is the peak signal-to-noise ratio (PSNR), which is defined based on the mean square error (MSE) where x is the reconstructed image, y is the reference image, N is the number of pixels, and MAX is the maximum pixel value. PSNR has a unit of decibel (dB), and a larger value means a less image distortion.

$$\begin{cases} \mathrm{MSE}=\dfrac{1}{N}\sum\limits_{i}^{N}(x(i)-y(i))^2, \\ \mathrm{PSNR}=10\lg\left(\dfrac{\mathrm{MAX}^2}{\mathrm{MSE}}\right). \end{cases} \tag{8}$$

The second metric is SSIM, which can measure the similarity between two images by considering luminance l, contrast c, and structural information s, as follows:

$$\begin{cases} l(x,y)=\dfrac{2\mu_x\mu_y+C_1}{\mu_x^2+\mu_y^2+C_1}, \\ c(x,y)=\dfrac{2\sigma_x\sigma_y+C_2}{\sigma_x^2+\sigma_y^2+C_2}, \\ s(x,y)=\dfrac{\sigma_{xy}+C_3}{\sigma_x\sigma_y+C_3}, \\ \mathrm{SSIM}(x,y)=l(x,y)\cdot c(x,y)\cdot s(x,y), \end{cases} \tag{9}$$

where μ_x and σ_x are the mean and variance of image x, μ_y and σ_y are the mean and variance of image y, σ_{xy} is the covariance of x and y, and C_1, C_2, and C_3 are constants. The SSIM index gives a value ranging from 0 to 1 (a value that is closer to 1 denotes a higher image similarity).

The third metric is the relative L2 norm error (RLNE), which is used to evaluate reconstruction error as Eq. (10). The smaller the value of RLNE is, the smaller the reconstruction error will be.

$$\mathrm{RLNE}=\frac{\|\boldsymbol{x}-\boldsymbol{y}\|_2}{\|\boldsymbol{y}\|_2}. \tag{10}$$

In addition to image quality comparison, the computational cost of the proposed method was evaluated in our study. All experiments were implemented using MATLAB 2014b and run on a PC with an Intel Core i5-6500 CPU@3.2 GHz and 8 GB memory.

3.2 Performance evaluation on digital phantom

In the digital phantom study, the original phantom data were directly used as the ground-truth image. As mentioned in Section 1, low-dose CT can be implemented by lowering tube current or reducing projection views. To have a more comprehensive study, we tested our method in both a low-current case and a few-view case.

In the low-current case, CT scan dose was set to $\boldsymbol{I}_0=5\times10^3$ photons per ray and 364 projections over 360° were simulated. The imaging results of different methods are shown in Fig. 2. It can be seen that the FBP result in Fig. 2b contains heavy noise in the whole reconstructed region. Even worse, some small structures are almost covered by noise, which will cause misdiagnosis in the clinic. As shown in Fig. 2c, the image becomes much cleaner after being denoised by BM3D, but the edges in the image are seriously blurred compared to that in the ground-truth image in Fig. 2a. Fig. 2d shows the image reconstructed by SART, which maintains better details than FBP-BM3D, but has less smoothing effect. As we can see in Fig. 2e, the CS-based iterative method ABOCS effectively suppresses noise and artifacts. Fig. 2f shows that the proposed method achieves a little better noise reduction and more recognizable structures than ABOCS.

In the few-view case, CT scan dose was set to a clinical level, $\boldsymbol{I}_0=5\times10^4$ photons per ray, and the number of projections was down-sampled to 91. Imaging results of different methods are presented in Fig. 3. Obviously, the reconstructed image of FBP in Fig. 3b contains unacceptable noise and streak

artifacts. As seen in Fig. 3c, BM3D is still effective in reducing noise as in the low-current case, but achieves little effect in reducing streak artifacts. Fig. 3d shows that SART merely smooths the image, but a lot of streak artifacts can still be identified. ABOCS reconstructs a far better image as shown in Fig. 3e, but its image still contains a little visible unwanted texture. In contrast, it is easy to see in Fig. 3f that our method outperforms all the other methods, obtaining an image with the finest details and the least noise and artifacts.

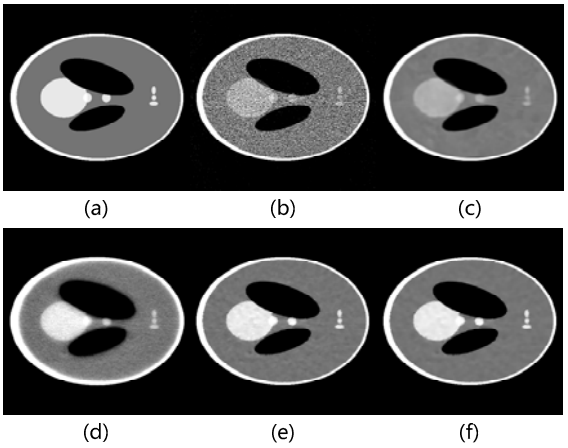

Fig. 2 Imaging results of different methods for low-current case on Shepp-logan: (a) ground-truth image; (b) FBP; (c) FBP-BM3D; (d) SART; (e) ABOCS; (f) proposed method (display window is [−250, 300] HU)

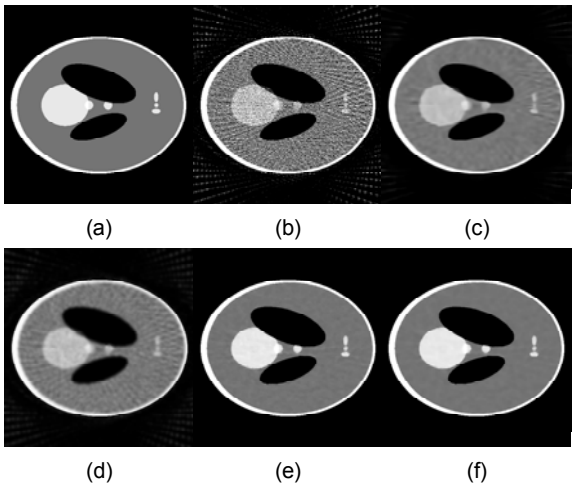

Fig. 3 Imaging results of different methods for few-view case on Shepp-logan: (a) ground-truth image; (b) FBP; (c) FBP-BM3D; (d) SART; (e) ABOCS; (f) proposed method (display window is [−250, 300] HU)

The quantitative assessment was carried out by calculating PSNR, SSIM, and RLNE between the ground-truth image and reconstructed images. Table 1 lists the performance comparison of different methods. Clearly, FBP yields low image quality in terms of all three metrics. The following columns of Table 1 demonstrate that FBP-BM3D and SART also fail to present satisfactory numeric results, while only ABOCS and the proposed method achieve satisfactory results. Note that whether we consider PSNR, SSIM, or RLNE, the proposed method obtains a comparable result with ABOCS, enjoying an up to 1.6% enhancement.

Table 1 Numeric results on Shepp-logan

Case	Index	FBP	FBP-BM3D	SART	ABOCS	Proposed
Low-current	PSNR	12.308	23.678	18.667	**28.980**	28.860
	SSIM	0.6050	0.9561	0.7136	0.9475	**0.9627**
	RLNE	0.6083	0.1697	0.3021	**0.0922**	0.0933
Few-view	PSNR	12.800	24.603	18.062	30.259	**30.320**
	SSIM	0.3729	0.8365	0.6510	0.9732	**0.9833**
	RLNE	0.5949	0.1526	0.3238	0.0796	**0.0791**

The best results are typed in bold fonts. PSNR: peak signal-to-noise ratio, unit is dB; SSIM: structural similarity; RLNE: relative L2 norm error; FBP: filtered backprojection; FBP-BM3D: filtered backprojection block matching; SART: simultaneous algebraic reconstruction technique; ABOCS: accelerated barrier optimization compressed sensing

3.3 Performance evaluation on physical phantom

In the physical phantom study, image reconstructed from 655 projections acquired under an 80-mA tube current was used as the ground-truth image. To further evaluate the proposed method, we investigated a much worse case, where the tube current was lowered to 40 mA and the number of projections was undersampled to 66.

Results are shown in Fig. 4. In the FBP image (Fig. 4b), some small structures are overwhelmed by noise and streak artifacts. In the FBP-BM3D image (Fig. 4c), some small structures are almost wiped out. SART introduces arc-shaped artifacts that result in a significant damage in the image (Fig. 4d). As shown in Figs. 4e and 4f, ABOCS and the proposed method achieve acceptable results, and the proposed method still surpasses ABOCS because of a lower noise level and fewer artifacts.

Table 2 compares the numeric results of these methods. Both FBP and SART achieve poor results with the value below 0.5 for SSIM. FBP-BM3D

obtains a high PSNR over 30 dB, but this good numeric result does not make sense because of the oversmoothed image and smeared details shown in Fig. 4c. It is worth noting that the proposed method obtains the best results in all numeric metrics.

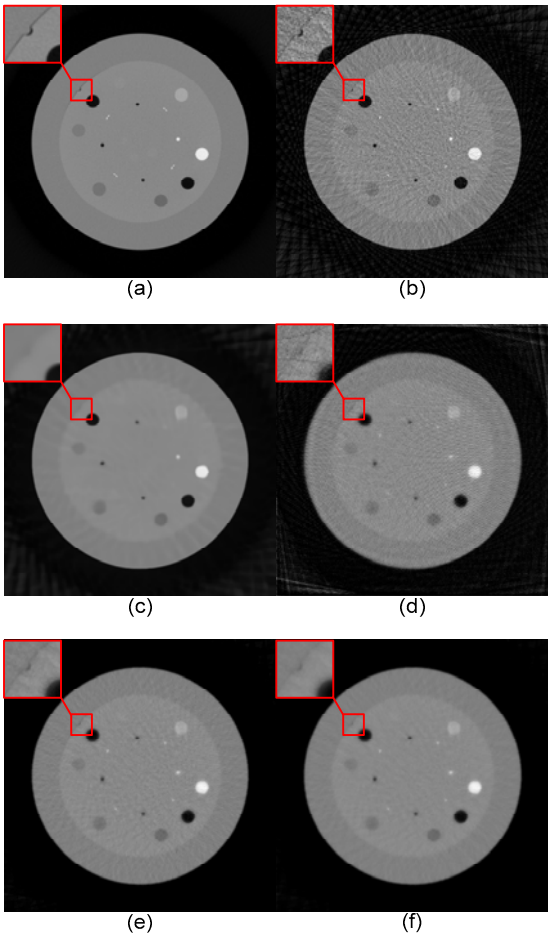

Fig. 4 Imaging results of different methods on Catphan: (a) ground-truth image; (b) FBP; (c) FBP-BM3D; (d) SART; (e) ABOCS; (f) proposed method (display window is [−1000, 1000] HU)

Table 2 Numeric results on Catphan

Index	FBP	FBP-BM3D	SART	ABOCS	Proposed
PSNR	22.814	30.709	22.396	30.890	**31.560**
SSIM	0.3352	0.6728	0.4463	0.7738	**0.8114**
RLNE	0.1978	0.0798	0.2076	0.0781	**0.0698**

The best results are typed in bold fonts. Unit for PSNR is dB

3.4 Imaging performance discussion and computational cost evaluation

According to the above experimental results, analytical reconstruction represented by FBP produces unacceptable images in both the low-current case and few-view case, confirming that FBP is not suitable for low-dose reconstruction (Han *et al.*, 2012). The terrible results of SART indicate that classical iterative reconstruction is also not able to resolve low-dose CT problems. The experiments verify that BM3D is really effective in image denoising, but it has fatal drawbacks. First, as shown in Figs. 2c, 3c, and 4c, BM3D tends to excessively smooth the images, leading to blurred edges. Second, especially for the few-view case, BM3D fails to handle streak artifacts, possibly because BM3D is not theoretically designed for artifact correction. In clinical use, FBP-BM3D may smear some critical tissues and mislead diagnosis made by doctors, and thus can hardly be adopted for low-dose CT reconstruction. In our study, only ABOCS and the proposed method achieve satisfactory results. Notably, the proposed method outperforms ABOCS in both qualitative and quantitative evaluation.

Improvement of image quality is not enough; we should also consider the execution time. Because the former three methods are not acceptable for clinical use, it is meaningless to consider their computational efficiencies. Fig. 5 compares the computational cost of ABOCS and the proposed method in the low-current case and few-view case. Compared with ABOCS, the proposed method realizes an almost threefold speed-up because of the significant reduction of iterations.

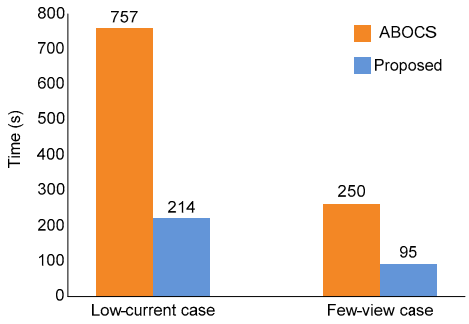

Fig. 5 Comparison of computational cost for ABOCS and the proposed method

4 Conclusions

We have presented a novel solution for low-dose CT reconstruction by combining TV minimization and sparse dictionary learning. Experiments revealed that the proposed method achieves much better

imaging results than analytical algorithm FBP, conventional iterative reconstruction SART, and a typical CS-based reconstruction method ABOCS. Specifically, compared with ABOCS, the proposed method maintains better image quality while reducing time overhead. The superior performance of our method demonstrates its power and potential for low-dose CT reconstruction. Future work may employ parallel computing platforms to further accelerate the reconstruction.

References

Aharon, M., Elad, M., Bruckstein, A.M., 2006. The K-SVD: an algorithm for designing of overcomplete dictionaries for sparse representation. *IEEE Trans. Signal Process.*, **54**(11):4311-4322. https://doi.org/10.1109/TSP.2006.881199

Anderson, A.H., Kak, A.C., 1984. Simultaneous algebraic reconstruction technique (SART): a superior implementation of the ART algorithm. *Ultrason. Imag.*, **6**(1):81-94. https://doi.org/10.1177/016173468400600107

Barzilai, J., Borwein, J., 1988. Two-point step size gradient methods. *IMA J. Numer. Anal.*, **8**(1):141-148. https://doi.org/10.1093/imanum/8.1.141

Candes, E.J., Romberg, J., Tao, T., 2006. Robust uncertainty principles: exact signal reconstruction from highly incomplete frequency information. *IEEE Trans. Inform. Theory*, **52**(2):489-509. https://doi.org/10.1109/TIT.2005.862083

Chen, Y., Shi, L.Y., Feng, Q.J., *et al.*, 2014. Artifact suppressed dictionary learning for low-dose CT image processing. *IEEE Trans. Med. Imag.*, **33**(12):2271-2292. https://doi.org/10.1109/TMI.2014.2336860

Dabov, K., Foi, A., Katkovnik, V., *et al.*, 2007. Image denoising by sparse 3-D transform-domain collaborative filtering. *IEEE Trans. Image Process.*, **16**(8):2080-2095. https://doi.org/10.1109/TIP.2007.901238

Dong, W.S., Zhang, L., Shi, G.M., *et al.*, 2013. Nonlocally centralized sparse representation for image restoration. *IEEE Trans. Image Process.*, **22**(4):1620-1630. https://doi.org/10.1109/TIP.2012.2235847

Elad, M., Aharon, M., 2006. Image denoising via sparse and redundant representations over learned dictionaries. *IEEE Trans. Image Process.*, **15**(12):3736-3745. https://doi.org/10.1109/TIP.2006.881969

Ginat, D.T., Gupta, R., 2014. Advances in computed tomography imaging technology. *Ann. Rev. Biomed. Eng.*, **16**:431-453. https://doi.org/10.1146/annurev-bioeng-121813-113601

Han, X., Bian, J.G., Ritman, E.L., *et al.*, 2012. Optimization-based reconstruction of sparse images from few-view projections. *Phys. Med. Biol.*, **57**(16):5245-5273. https://doi.org/10.1088/0031-9155/57/16/5245

Jia, X., Dong, B., Lou, Y.F., *et al.*, 2011. GPU-based iterative cone-beam CT reconstruction using tight frame regularization. *Phys. Med. Biol.*, **56**:3787-3807. https://doi.org/10.1088/0031-9155/56/13/004

Liu, J., Chen, Y., Hu, Y., *et al.*, 2016. Low-dose CBCT reconstruction via 3D dictionary learning. IEEE 13th Int. Symp. on Biomedical Imaging, p.735-738. https://doi.org/10.1109/ISBI.2016.7493371

Lustig, M., Donoho, D.L., Santos, J.M., *et al.*, 2008. Compressed sensing MRI. *IEEE Signal Process. Mag.*, **25**(2): 72-82. https://doi.org/10.1109/MSP.2007.914728

Niu, T.Y., Zhu, L., 2012. Accelerated barrier optimization compressed sensing (ABOCS) reconstruction for cone-beam CT: phantom studies. *Med. Phys.*, **39**(7):4588-4598. https://doi.org/10.1118/1.4729837

Niu, T.Y., Ye, X.J., Fruhauf, Q., *et al.*, 2014. Accelerated barrier optimization compressed sensing (ABOCS) for CT reconstruction with improved convergence. *Phys. Med. Biol.*, **59**(7):1801-1814. https://doi.org/10.1088/0031-9155/59/7/1801

Park, J.C., Song, B.Y., Kim, J.S., *et al.*, 2012. Fast compressed sensing-based CBCT reconstruction using Barzilai-Borwein formulation for application to on-line IGRT. *Med. Phys.*, **39**(3):1207-1217. https://doi.org/10.1118/1.3679865

Siddon, R.L., 1985. Prism representation: a 3D ray-tracing algorithm for radiotherapy application. *Phys. Med. Biol.*, **30**:817-824. https://doi.org/10.1088/0031-9155/30/8/005

Sidky, E.Y., Kao, C.M., Pan, X.C., 2008. Image reconstruction in circular cone-beam computed tomogrphy by constrained, total-variation minimization. *Phys. Med. Biol.*, **53**:4777-4807. https://doi.org/10.1088/0031-9155/53/17/021

Wang, Z., Bovik, A.C., Sheikh, H.R., *et al.*, 2004. Image quality assessment: from error visibility to structural similarity. *IEEE Trans. Image Process.*, **13**(4):600-612. https://doi.org/10.1109/TIP.2003.819861

Xu, Q., Yu, H.Y., Mou, X.Q., *et al.*, 2012. Low dose X-ray reconstruciton via dictionary learning. *IEEE Trans. Med. Imag.*, **31**(9):1682-1697. https://doi.org/10.1109/TMI.2012.2195669

Yan, H., Cervino, L., Jia, X., *et al.*, 2012. A comprehensive study on the relationship between the image quality and imaging dose in low-dose cone beam CT. *Phys. Med. Biol.*, **57**(7):2063-2080. https://doi.org/10.1088/0031-9155/57/7/2063

Yan, H., Wang, X.Y., Shi, F., *et al.*, 2014. Towards the clinical implementation of iterative low-dose cone-beam CT reconstruction in image-guided radiation therapy: cone/ring artifact correction and multiple GPU implementation. *Med. Phys.*, **41**(11):1-15. https://doi.org/10.1118/1.4898324

Yu, H.Y., Wang, G., 2010. A soft-threshold filtering approach for reconstruction from a limited number of projections. *Phys. Med. Biol.*, **55**:3905-3916. https://doi.org/10.1088/0031-9155/55/13/022

Yuan, M., Yang, B.X., Ma, Y.D., *et al.*, 2015. Multi-scale UDCT dictionary learning based highly undersampled MR image reconstruction using patch-based constraint splitting augmented Lagrangian shrinkage algorithm. *Front. Inform. Technol. Electron. Eng.*, **16**(2):1069-1087. https://doi.org/10.1631/FITEE.1400423